Journal of Solid State Chemistry **165,** 19–24 (2002)
doi:10.1006/jssc.2001.9484, available online at http://www/idealibrary.com on IDEAL®

Luminescence Properties of Terbium-, Cerium-, or Europium-Doped α-Sialon Materials

J. W. H. van Krevel,* J. W. T. van Rutten,* H. Mandal,† H. T. Hintzen,*,[1] and R. Metselaar*

*Laboratory of Solid State and Materials Chemistry, Eindhoven University of Technology, P.O. Box 513, 5600 MB Eindhoven, The Netherlands; and †Department of Ceramics Engineering, Anadolu University, Eskisehir 26470, Turkey
E-mail: h.t.hintzen@tue.nl

Received September 1, 2000; in revised form November 22, 2001; accepted December 21, 2001

New interesting luminescent α-sialon ($M^{val+}_{(m/val+)}$ $Si_{12-(m+n)}Al_{(m+n)}O_nN_{(16-n)}$) ($M$ = Ca, Y) materials doped with Ce, Tb, or Eu have been prepared and their luminescence properties studied. These show that Tb and Ce are in the 3+ and Eu in the 2+ state. Low-energy $4f \leftrightarrow 5d$ transitions are observed as compared to the luminescence of these ions doped in oxidic host-lattices. This is partially explained by the nitrogen-rich coordination of the rare-earth ion and partially by the narrow size of the lattice site. The latter gives rise to a strong crystal-field splitting of the 5*d* band and a rather large Stokes shift for Ce^{3+} and Eu^{2+} (6500–7500 and 7000–8000 cm^{-1}, respectively). For (Y,Tb)-α-sialon the Tb^{3+} $4f \rightarrow 5d$ excitation band ($\sim$260 nm) is in the low-energy host-lattice absorption band ($\leq$290 nm), giving rise to a strong absorption for 254-nm excitation, but a low quantum efficiency. The latter is due to photoionization processes or selective excitation of Tb^{3+} at the defect-rich surface, resulting in radiationless transitions. Ce- and Eu-doped Ca–α-sialon show bright long-wavelength luminescence (maxima at 515–540 and 560–580 nm for Ce and Eu, respectively) with a high quantum efficiency and high absorption for 365- and 254-nm excitation. The Eu^{2+} emission intensity and absorption increases for increasing *m*, which is explained by the Eu^{2+} richer α-sialon composition. The position of the Eu^{2+} emission does not shift with changing composition of the host-lattice (*m*, *n* values), indicating that the local coordination of the Eu^{2+} ion is hardly dependent on the matrix composition. © 2002 Elsevier Science (USA)

Key Words: **terbium; europium; cerium; luminescence; oxynitride, SiAlON.**

1. INTRODUCTION

M–α-sialon ($M^{val+}_{(m/val+)}$ $Si_{12-(m+n)}Al_{(m+n)}O_nN_{(16-n)}$, where val is the valence of the metal ion) can be deduced from α-Si_3N_4, in which *M* is a metal ion, such as Li^+, Ca^{2+}, Y^{3+} (1) or a rare-earth ion (2). In this structure Si–N is partially replaced by Al–O (*n*) or Al–N (*m*). In the latter case, the charge difference is compensated for by the incorporation of metal ions. *M*–α-sialon has intensively been studied for its attractive mechanical properties and stability at higher temperatures (2–5).

Rare-earth ions are known to give efficient luminescence and, e.g., rare-earth-doped phosphors are applied in fluorescent lamps or in cathode ray tubes (6–7). Until now nothing has been reported concerning the luminescence properties of the rare-earth ions, doped in the *M*–α-sialon matrix, although it can result in an interesting phosphor material. Further, only little has been reported on the optical properties in general, such as absorption spectra, of rare-earth–α-sialon materials (8, 9). In addition, the chemical composition of *M*–α-sialon (i.e., *m* and *n*) can be altered over a broad range without changing the crystal structure, which makes it possible to adjust the properties.

For the ions Ce^{3+}, Tb^{3+}, and Eu^{2+} efficient absorption of radiation occurs by $4f \rightarrow 5d$ transitions, which are normally in the UV part of the spectrum (7). Recently, we reported on the luminescence of Ce^{3+} and Tb^{3+} in different Y–Si–O–N compounds and observed shifts of the $4f \rightarrow 5d$ transitions to lower energy when the nitrogen content increases. This was explained by two factors (10, 11).

* The center of gravity shifts toward lower energy when Ce^{3+}/Tb^{3+} coordinates to the less electronegative nitrogen compared to oxygen, which causes an increase in covalency (nephelauxetic effect).

* The ligand-field splitting of the 5*d* band increases when more N^{3-} versus O^{2-} coordinates to the lanthanide ion. This is caused by the higher formal charge of N^{3-} compared to O^{2-}.

In addition, for the Ce^{3+}-doped materials we also observed that the Stokes shift decreases for Y–Si–O–N lattices with a higher nitrogen concentration. This is ascribed to the increasing rigidity of the host-lattice as a result of a more extended silicon tetrahedral network in

[1]To whom correspondence should be addressed.

0022-4596/02 $35.00
© 2002 Elsevier Science (USA)
All rights reserved.

this sequence (10). For the Tb^{3+}-doped *Ln*–Si–O–N samples (*Ln* = Y, Gd, and La) it was shown that efficient absorption of radiation takes place by low-energy Tb^{3+} 5*d* bands overlapping the host-lattice absorption edge. It results in highly efficient green emission for 254-nm excitation (11).

In *M*–α-sialon the *M* cation is coordinated by seven (N,O) anions at three different *M*–(N,O) distances (Fig. 1, (12)). The *M*–(O,N) (2) bond is much shorter than the other six *M*–(O,N) bonds. This type of sevenfold coordination favors incorporation of the smaller alkaline-earth and rare-earth cations. The size of this *M* cation site is dominated by the $(Si, Al)_{12}(O,N)_{16}$ network, as demonstrated by almost the same average *M*–(N,O) distances found for Ca–α-sialon and Y–α-sialon (13), independent of the difference in ionic radius between Ca^{2+} (1.06 Å) and Y^{3+} (0.96 Å). Neutron diffraction did not yield unambiguous information about possible O/N ordering around the *M* cation, as the oxygen concentration was too low to detect a site preference for this ion (14). EXAFS results obtained for Er–α-sialon (15) and Yb–α-sialon (16) show that two out of the seven anionic positions are preferentially occupied by oxygen ions while the other coordinating positions are occupied by nitrogen ions, indicating an O/N ratio around the metal ion higher than the average matrix value. Because of the small cation site, the metal cation evidently prefers coordination with more smaller O anions than the large N anions, as compared to that expected from the average O/N ratio.

Almost single-phase *M*–α-sialon is obtained when *M* is a small ion, such as the smaller alkaline (earth) metals Li, Mg, or Ca or the smaller rare-earth ions Y or Yb–Sm ($\leq$1 Å), among which is Tb^{3+}. In agreement with this, single-phase Tb–α-sialon has been reported (8). Therefore, the preparation of the Tb-doped Y–α-sialon will pose no problem.

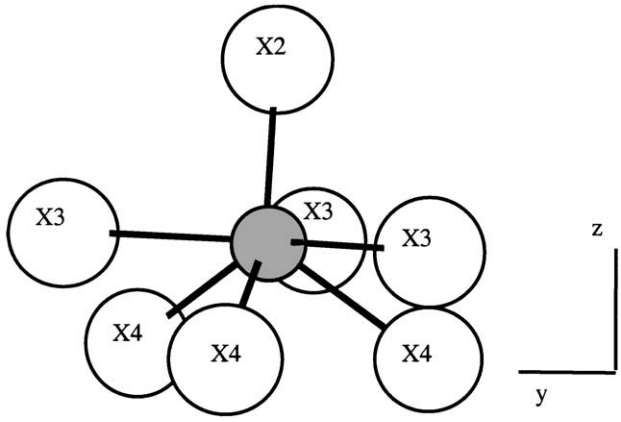

FIG. 1. Sevenfold coordination of the *M* cation in *M*–α-sialon. The gray sphere represents the M^{n+} ion. The white spheres (X2–X3–X4) are the three different crystallographic sites for the N/O anions.

From a size point-of-view it would be possible that Eu incorporates into the α-sialon lattice when it is in the 3+ state, since the radius of Eu^{3+} is in the range of neighboring rate-earth(III) ions (Sm and Gd), for which single-phase α-sialon was reported (2, 8). According to Shen *et al.* Eu^{3+}–α-sialon does indeed exist (8, 17, 18), but single phase could not be obtained due to partial reduction of Eu^{3+} to the divalent state. It is postulated that the resulting Eu^{2+} ion is too large to enter the α-sialon structure (8, 17, 18).

For the larger rare-earth ion Ce^{3+} ($\sim$1.1 Å), single-phase α-sialon materials have until now not been reported (19, 20). However, by applying a mixture of Y and Ce ions, it has been shown that small amounts of Ce^{3+} can be incorporated into the lattice (21–23). Very recently, preparation of almost 100% pure α-sialon, containing a considerable amount of Ce in combination with Ca and Yb has been reported (24, 25).

In this paper we report about the luminescence properties of Eu-, Ce-, and Tb-doped Y– and Ca–α-sialon and the influence of compositional variations.

2. EXPERIMENTAL

The powders $(Y_{0.9}Ce_{0.1})$–α-sialon and $(Y_{0.9}Tb_{0.1})$–α-sialon were of weighed-out composition $m = 1.5$ and $n = 1.5$. For $(Ca_{0.98}Eu_{0.02})$–α-sialon powder several compositions with $m = 0.5$–3 and $n = 0$–2.5 were chosen. Starting powders were α-Si_3N_4 (Starck LC12), γ-Al_2O_3 (AKPG and Sumitomo), AlN (Starck Grade C), Y_2O_3 (Rhône-Poulenc, 99.999%), $CaCO_3$ (Merck, p.a.), Ca_3N_2 (Johnson Mattey GmbH, 98%), Tb_4O_7 (Philips Maarheze, 99.999%), CeO_2 (Rhône-Poulenc, 99.95%), and Eu_2O_3 (Rhône-Poulenc, 99.99%). The raw materials were weighed out stoichiometrically. Next, they were suspended in *i*-propanol, and mixed on a roller-bench for 48 h using Si_3N_4 balls. The resulting mixture was dried and fired in Mo crucibles under a 5% H_2/95% N_2 atmosphere for about 2 h at 1700°C and cooled at a rate of 3°C/min. After firing, the obtained samples were ground to obtain a fine powder. A dense transparent $(Ca_{0.3125}Ce_{0.209})$–α-sialon ($m = 1.25$, $n = 1.15$) ceramic was prepared as described in Ref. (25).

X-ray powder diffraction with Cu*K*α radiation (Philips PW 1120 or Rigaku) showed that α-sialon phase was obtained for all samples with only a minimal amount of secondary phase. Luminescence spectra of all samples and diffuse reflection spectra of the powders were obtained, using a Perkin-Elmer LS 50 B spectrophotometer. For correction of the excitation spectra with respect to the lamp intensity part of the excitation beam was led to a second photomultiplier via a beam-splitter. Correction of the emission spectra between 340 and 900 nm was performed by dividing the measured emission spectrum by the ratio of

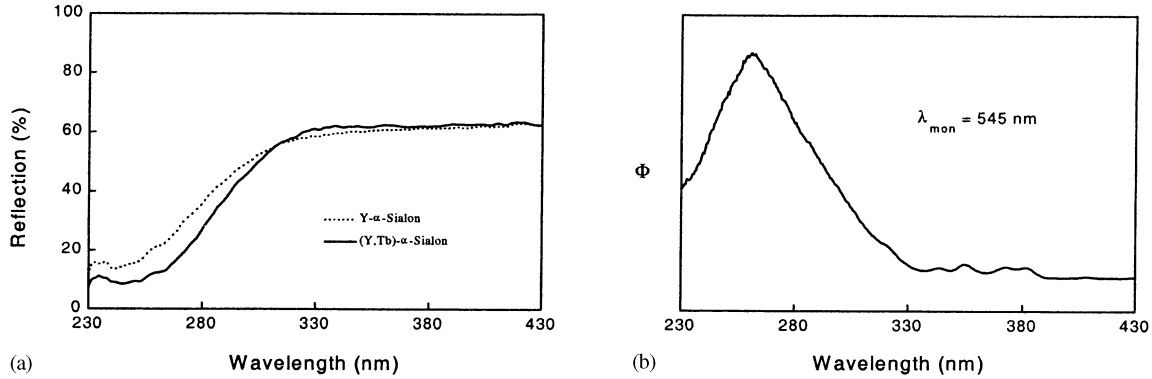

FIG. 2. (a) Reflection spectrum of $Y_{0.5}Si_9Al_3O_{1.5}N_{14.5}$ and $Y_{0.45}Tb_{0.05}Si_9Al_3O_{1.5}N_{14.5}$; (b) excitation spectrum of $Y_{0.45}Tb_{0.05}Si_9Al_3O_{1.5}N_{14.5}$.

the observed spectrum of a calibrated W-lamp and its known spectral distribution.

3. RESULTS AND DISCUSSION

3.1. Tb-Doped α-Sialon

Undoped as well as Tb-doped Y–α-sialon are white powders and show strong absorption in the UV part of the spectrum (290 nm, Fig. 2a). The drop in the reflection spectrum is almost the same for both and therefore attributed to host-lattice absorption. It starts below 320 nm (Fig. 2a and Table 1). In agreement with these observations, an increase at about the same position was observed in the absorption spectrum, reported by Shen *et al.*, for both Tb– and Y–α-sialon ceramic (8).

Under 254-nm excitation, the 10 at.% doped Tb sample shows green–yellow luminescence, which originates from $4f$–$4f$ transitions, typical for Tb^{3+} ($^5D_4 \rightarrow {}^7F_j$). The corresponding excitation band has its maximum at about 260 nm (Fig. 2b, Table 1). Similar broadbands in the UV part of the spectrum have also been observed for Tb^{3+} in other systems and originate from $4f^8 \rightarrow 4f^7 5d$ transitions (7, 26). Therefore, we attribute them to these transitions. The position of the excitation band is at a relatively low energy, which is also expected for Tb^{3+}, present in the nitrogen-rich environment of the α-sialon matrix (11).

The position of the excitation band (260 nm) matches very well with the 254-nm radiation, which is applied in mercury discharge lamps. Further, the 254-nm absorption is strong (about 90%, Fig. 2a) for $(Y_{0.9}Tb_{0.1})$–α-sialon, as a result of host-lattice absorption. However, the relative emission intensity of $(Y_{0.9}Tb_{0.1})$–α-sialon is lower than that of $(Y_{0.9}Tb_{0.1})_2Si_3O_3N_4$ (quantum efficiency about 20%, UV absorption about 90% (11)), indicating that the quantum efficiency is below 20%. A similar behavior was also observed for host-lattice excitation of Y–Si–O–N:Tb compounds (11). These low quantum efficiencies are ascribed to the possible occurrence of photoionization processes (due to the Tb $5d$ band in the host-lattice band), or selective excitation of Tb^{3+} ions at the defect rich powder particle surface (due to a small penetration depth for strong host-lattice absorption), resulting in radiationless transitions. For the low quantum efficiency of $(Y_{0.9}Tb_{0.1})$–α-sialon, the same explanation can be given.

3.2. Ce-Doped α-Sialon

It is striking that the luminescence properties of the Ce-doped Y–α-sialon materials are completely different from those of the Ce-doped Ca–α-sialon sample (Table 1). The

TABLE 1
The Color, Absorption Edge, Emission Color for Irradiation by 254 nm/365 nm, Excitation Maxima (nm), Emission Maxima (nm), and the Stokes Shift (cm^{-1}) of the Undoped and Rare-Earth-Doped α-Sialon Samples

	Y powder	$Y_{0.9}Tb_{0.1}$ powder	$Y_{0.9}Ce_{0.1}$ powder	Ca powder	$Ca_{0.3125}Ce_{0.209}$ ceramic	$Ca_{0.98}Eu_{0.02}$ powder
Day light color	White	White	White	White	Yellow	Yellow
Absorption edge[a] (nm)	~290	~290	—	~260	—	~540
Emission color	—	Yellow–green	Blue	—	Green–yellow	Bright yellow
Excitation maxima (nm)	—	~260	~280	—	~275	~310
			~340	—	~385	~400
Emission maximum (nm)	—	~545 (line)	430–460 (band)	—	515–540 (band)	560–580 (band)
Stokes shift (cm^{-1})	—	—	~7000	—	6500–7500	7000–8000

[a]Obtained from diffuse reflection spectrum.

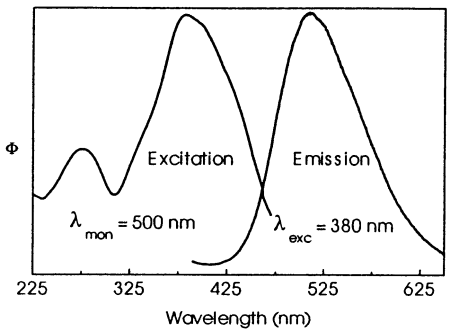

FIG. 3. Excitation and emission spectrum of $Ca_{0.3125}Ce_{0.209}Si_{9.6}Al_{2.4}O_{1.15}N_{14.85}$.

emission and excitation spectra of Ce-doped Y–α-sialon are typical for an oxidic host-lattice, as compared to the red-shifted spectra observed for Ce-doped Ca–α-sialon. From this we conclude that Ce is negligibly incorporated into the Y–α-sialon matrix, which is in agreement with literature data (21–23). In contrast to Y–α-sialon, a large amount of Ce can incorporate into the Ca–α-sialon matrix, as was shown by one of us recently (24, 25). Therefore, we continued with the $(Ca_{0.3125}Ce_{0.209})$–α-sialon sample. $(Ca_{0.3125}Ce_{0.209})$–α-sialon is yellow and shows a bright green–yellow emission under irradiation with UV light (Fig. 3 and Table 1). The yellow daylight color originates from absorption by Ce^{3+} in the blue part of the spectrum (400–480 nm). This absorption leads to efficient luminescence, as can be seen from the excitation spectrum (Fig. 3 and Table 1). The Ce^{3+} excitation and emission bands for (Ca,Ce)–α-sialon are at a longer wavelength than normally observed for oxidic materials (7). These long-wavelength Ce^{3+} excitation and emission bands are an indication that the Ce^{3+} coordination is nitrogen rich and confirms that Ce^{3+} is incorporated into the α-sialon matrix. The low-energy excitation bands are the result of a center of gravity at low energy and a strong crystal-field splitting due to coordination with nitrogen, as found earlier by us for Ce-doped Y–Si–O–N compounds (10). The large-crystal-field splitting is further enlarged by the small size of the metal site in the α-sialon matrix, on which Ce^{3+} is substituted. For Ce^{3+}, incorporated into the rigid 3-dimensional Si–Al–O–N network of the α-sialon structure, we would expect a small Stokes shift ($<4000\,cm^{-1}$ (10)). However, the observed Stokes shift is quite large (about 6500–$7500\,cm^{-1}$). The difference must be explained by the small size of the metal site in the α-sialon matrix. This promotes shrinkage of the Ce^{3+} ion in the excited state compared to the ground state (27), resulting in a large relaxation and thus a large Stokes shift.

Depending on the excitation wavelength, an emission band with a maximum varying between about 515–540 nm is observed. Emission near 540 nm is particularly observed when excitation occurs above 400 nm. Simultaneously, for monitoring wavelengths longer than 540 nm, a shoulder between 425 and 475 nm appears in the excitation spectrum of the Ce-doped ceramic. In our opinion these small changes in emission and excitation spectra for different excitation and monitoring wavelengths, respectively, may originate from some variation in the coordination of Ce^{3+} due to the presence of structural defects related with the incorporation of the large Ce^{3+} ion into the α-sialon lattice (23).

When a comparison is made between the position of the lowest excitation band of Tb^{3+} (about 260 nm, Fig. 2b) and Ce^{3+} (about 385 nm, Fig. 3), we observe a difference in energy of 12,000–$13,000\,cm^{-1}$. This value agrees with the energy differences we have found for Ce/Tb-doped Y–Si–O–N materials (10) and literature data for other compounds (28).

3.3. *Eu-Doped α-Sialon*

Undoped Ca–α-sialon is a white powder, which shows absorption in the UV part of the spectrum (absorption edge near 260 nm, Fig. 4a). Eu-doped Ca–α-sialon powder, on the other hand, is yellow. The reflection spectrum of Eu-doped α-sialon (Fig. 4b) extends to the blue part of the spectrum (400–500 nm), which explains the yellow color. The emission band is broad, which is characteristic of the

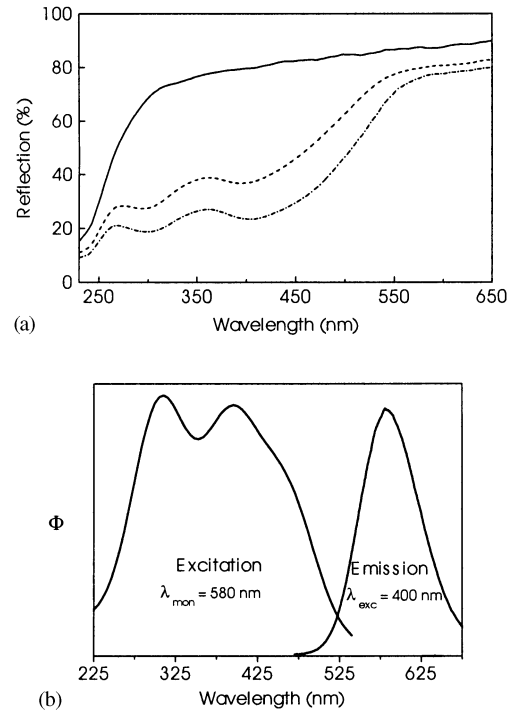

FIG. 4. (a) Reflection spectra of $CaSi_{10}Al_2N_{16}$ (solid line), $Ca_{0.98}Eu_{0.02}Si_{10}Al_2N_{16}$ (dashed line), and $Ca_{1.47}Eu_{0.03}Si_9Al_3N_{16}$ (dash-dotted line); (b) excitation and emission spectra of $Ca_{1.47}Eu_{0.03}Si_9Al_3N_{16}$.

$5d \rightarrow 4f$ transition of Eu^{2+}. We could not detect the Eu^{3+} line emission (590–615 nm), nor did we observe absorption, which is typical for the presence of Eu^{3+}. This indicates that Eu^{3+} is not present. The Eu^{2+} luminescence is very efficient: for $Ca_{0.98}Eu_{0.02}Si_{10}Al_2N_{16}$ bright emission is observed for 365-nm excitation, combined with a strong absorption (70%), while for 254-nm excitation the intensity is lower.

The Eu^{2+} emission is at a wavelength (560–580 nm, Fig. 4b) much longer than normally observed (350–500 nm) (7). This effect is similar to the position of the $4f \leftrightarrow 5d$ transitions of Tb^{3+} and Ce^{3+}, which are also at longer wavelengths than generally found. The long-wavelength excitation and emission bands of Eu^{2+} suggest a nitrogen-rich coordination with a center of gravity at low energy and a large-crystal-field splitting. From the emission at 580 nm and the corresponding excitation spectrum, we can calculate that the Stokes shift is rather large (7000–8000 cm^{-1}), which was also the case for Ce^{3+} in α-sialon. The similarities in luminescence between Eu^{2+}, Tb^{3+}, and Ce^{3+} are a strong indication that the large Eu^{2+} ion is incorporated on a small nitrogen-rich site in the Ca–α-sialon matrix. In full agreement with this, for Sr^{2+}, with a radius comparably large to that of Eu^{2+}, a single-phase α-sialon is almost obtained, when Yb, Y, or Ca ions are present (24, 25, 29). In view of the above-mentioned results, we feel that in Eu–α-sialon, the Eu ion is present in its divalent state, in contrast to what has been recently suggested by Shen *et al.* (18). The fact that Eu–α-sialon is not formed as a single phase material (18) is in line with expectations of the similarity in ionic radius of Eu^{2+} and Sr^{2+}. For pure Sr^{2+} a single-phase Sr–α-sialon material was not obtained either (24, 25, 29, 30) and, in addition, the phase composition resembled that of Eu–α-sialon (30). Apparently, the presence of N^{3-} ions in the α-sialon matrix creates a driving force for reduction of Eu^{3+} to Eu^{2+}, a mechanism that was also demonstrated to occur in Eu-doped sialon glasses (31).

For varying compositions of the Eu-doped Ca–α-sialon lattice, we observed a change in cell parameters. For the m value, increasing from 0.5 to 3, the a axis varies from 7.80 to 7.93 Å and the c axis from 5.68 to 5.73 Å. For increasing n values we could not determine a significant change of the lattice parameters. The observed trends match those described in literature, where also the main effect is observed for increasing m value (32). For samples with compositions outside the single-phase Ca–α-sialon area ($m \leq 0.5$ or $n > 1.5$), apart from the yellow emission, assigned to Eu^{2+} in Ca–α-sialon, we observed a strong additional emission. This additional emission is in the blue–green part of the spectrum (420–520 nm) with corresponding excitation in the UV part of the spectrum. These luminescent centers are probably originating from Eu^{2+}, present in an oxygen-rich phase. Within the single phase α-sialon compositional region, the blue–green emission is weak and the yellow emission is dominant. The yellow Eu^{2+} emission becomes more intense for m values increasing from 0.5 to 3. From the reflection spectra it can be seen that the absorption becomes stronger (Fig. 4a), showing that for increasing m the total Eu^{2+} content increases. This can also be seen from the formula $M^{\text{val+}}_{(m/\text{val+})}Si_{12-(m+n)}Al_{(m+n)}O_nN_{(16-n)}$, showing that for increasing m more M and therefore also more ($Ca_{0.98}$, $Eu^{2+}_{0.02}$) are present in the lattice. Further significant differences in positions of Eu^{2+} emission and excitation bands could not be found for varying m and n. This indicates that, despite the variation in chemical composition of the host-matrix within the singe-phase α-sialon region, the local coordination of Eu^{2+} remains actually the same. Clearly, the Eu^{2+} ion dominates its local surroundings, as supported by the EXAFS measurements at Er– and Yb–α-sialon (15, 16). A negligible influence of the overall host-lattice composition on the local coordination of the luminescent ion was also observed for Ce-doped $Y_2Si_{3-x}Al_xO_{3+x}N_{4-x}$ with varying x (33).

4. CONCLUSIONS

We have prepared and characterized new interesting luminescent Ce-, Tb- or Eu-doped M–α-sialon (M = Ca or Y) materials. From luminescence measurements, we deduce that:

- Tb and Ce are present in the trivalent and Eu in the divalent state.
- Low-energy $4f \leftrightarrow 5d$ transitions are observed for Tb^{3+}, Ce^{3+}, and Eu^{2+}. This is explained by the nitrogen-rich environment, resulting in a center of gravity at low energy and a large-crystal-field splitting. Further, the small lattice site, on which Ce^{3+} and Eu^{2+} incorporate, enhances the crystal-field splitting and results in large Stokes shifts for both ions.
- The Tb^{3+}-doped sample has a low quantum efficiency and a high absorption for 254-nm excitation. This is explained by host-lattice absorption, resulting in photoionization or selective excitation of Tb^{3+} at the defect-rich surface, leading to radiationless transitions. The quantum efficiency and absorption of the Eu-doped samples are high for 365- and 254-nm excitation.
- The local coordination of the Eu^{2+} ion is not significantly influenced by the composition of the host-matrix.

ACKNOWLEDGMENTS

The authors highly appreciate the experimental contributions of C. Schreuders, B.J.F. Jakobs, and M.-E. Campos Castiñera and would acknowledge G. Bezemer for help with preparation of the samples.

REFERENCES

1. S. Hampshire, H. K. Park, and D. P. Thompson, *Nature* **274,** 880 (1978).
2. G. Z. Cao and R. Metselaar, *Chem. Mater.* **3,** 242 (1993) and references therein.
3. H. K. Park, D. P. Thompson, and K. H. Jack, *in* "Science of Ceramics," (H. Hausner, Ed.), Vol. 10, p. 251. Deutsche Keramische Gesellschaft, 1980.
4. H. Mandal, N. Camuscu, and D. P. Thompson, *J. Mater. Sci.* **30,** 5901 (1995).
5. T. Ekström, *J. Am. Ceram. Soc.* **75,** 259 (1992).
6. C. R. Ronda, T. Jüstel, and H. Nikol, *J. Alloys Compd.* **275–277,** 669 (1998).
7. G. Blasse and B. C. Grabmaier, "Luminescent Materials." Springer-Verlag, Berlin, 1994.
8. Z. Shen, M. Nygren, and U. Hålenius, *J. Mater. Sci. Lett.* **16,** 263 (1997).
9. B. S. B. Karunaratne, R. J. Lumby, and M.H. Lewis, *J. Mater. Res.* **11,** 2790 (1996).
10. J. W. H. van Krevel, H. T. Hintzen, R. Metselaar, and A. Meijerink, *J. Alloys Compd.* **268,** 272 (1998).
11. J. W. H. van Krevel, Ph.D. thesis, Eindhoven University of Technology, 2000.
12. F. Izumi, M. Mitomo, and J. Suzuki, *J. Mater. Sci. Lett.* **1,** 553 (1982).
13. F. Izumi, M. Mitomo, and Y. Bando, *J. Mater. Sci.* **19,** 3115 (1984).
14. G. Z. Cao, R. Metselaar, and W. G. Haije, *J. Mater. Sci. Lett.* 459 (1993).
15. M. Cole, K. P. J. O'Reilly, M. Redington, and S. Hampshire, *J. Mater. Sci.* **26,** 5143 (1991).
16. K. P. J. O'Reilly, M. Cole, S. Hampshire, and M. Redington, *J. Mater. Sci. Lett.* **12,** 271 (1993).
17. Z. Shen and M. Nygren, *Key Eng. Mater.* **132–136,** 755 (1997).
18. Z. Shen, M. Nygren, P. Wang, and J. Feng, *J. Mater. Sci. Lett.* **17,** 1703 (1998).
19. D. P. Thompson and H. Mandal, *Br. Ceram. Trans.* **96,** 199 (1997).
20. H. Mandal and D. P. Thompson, *J. Mater. Sci. Lett.* **15,** 1435 (1996).
21. T. Ekström, K. Jansson, P.-E. Olsson, and J. Persson, *J. Eur. Ceram. Soc.* **8,** 3 (1991).
22. E. Söderland and T. Ekström, *J. Mater. Sci.* **25,** 4815 (1990).
23. P.-E. Olsson, *J. Mater. Sci.* **24,** 3878 (1989).
24. H. Mandal, *in* "Conference and Exhibition of the ECerS," Bringhton, British Ceram. Proc. 60 Vol. 2, p. 11. Cambridge Univ. Press, Cambridge, UK, 1999.
25. H. Mandal, *J. Eur. Ceram. Soc.* **19,** 2349–2357 (1999).
26. G. Blasse and A. Bril, *Philips Res. Rep.* **2,** 481 (1967).
27. G. Blasse and A. Bril, *Philips, Tech. Rev.* **31,** 304 (1970).
28. M. J. J. Lammers and G. Blasse, *J. Electrochem. Soc.* **134,** 2068 (1987).
29. C. J. Hwang, D. W. Susnitzky, and D. R. Beaman, *J. Am. Ceram. Soc.* **78,** 588 (1995).
30. Z. Shen, J. Grins, S. Esmaeilzadeh, and M. Nygren, *in* "Conference and Exhibition of the ECerS," Brighton, British Ceram. Proc. 60, Vol. 2, p. 13. Cambridge Univ. Press, Cambridge, UK, 1999.
31. H. T. Hintzen, D. de Graaf, J. W. H. van Krevel, R. Metselaar, and G. De With, submitted.
32. J. W. T. van Rutten, H. T. Hintzen, and R. Metselaar, *J. Eur. Ceram. Soc.* **16,** 995 (1996).
33. J. W. H. van Krevel, H. T. Hintzen, and R. Metselaar, *Mater. Res. Bull.* **35,** 747 (2000).